Chinese Physics Letters

中国物理学会 Chinese Physical Society

Continuous-Wave Operation of Terahertz Quantum Cascade Lasers at 3.2 THz

To cite this article: Wang Tao *et al* 2013 *Chinese Phys. Lett.* **30** 064201

View the article online for updates and enhancements.

You may also like

- Preparation of patterned boron nanowire films with different widths of unit-cell and their field emission properties
Yong-Xin Zhang, , Fei Liu et al.
- High power-efficiency terahertz quantum cascade laser
Yuan-Yuan Li, , Jun-Qi Liu et al.
- Room-temperature continuous-wave interband cascade laser emitting at 3.45 m
Yi Zhang, , Fu-Hui Shao et al.

This content was downloaded from IP address 105.161.152.36 on 27/03/2023 at 08:03

CHIN. PHYS. LETT. Vol. 30, No. 6 (2013) 064201

Continuous-Wave Operation of Terahertz Quantum Cascade Lasers at 3.2 THz *

WANG Tao(王涛), LIU Jun-Qi(刘俊岐)**, CHEN Jian-Yan(陈剑燕), LIU Ying-Hui(刘颖慧), LIU Feng-Qi(刘峰奇)**, WANG Li-Jun(王利军), WANG Zhan-Guo(王占国)

Key Laboratory of Semiconductor Materials Science, Institute of Semiconductors, Chinese Academy of Sciences, Beijing 100083

(Received 5 January 2013)

We demonstrate continuous-wave (cw) operation of terahertz (THz) quantum cascade lasers emitting at 3.2 THz based on bound-to-continuum active region and semi-insulating surface-plasmon waveguide design. Optical power of 62 mW with a threshold current density of 285 A/cm^2 is obtained at 10 K from a 130-μm-wide and 1.5-mm-long laser in cw operation. Maximum cw operation temperature is up to 60 K. In pulsed mode, peak optical power more than 100 mW at 10 K and 2.1 mW at 85 K are observed from a 230-μm-wide and 2-mm-long device.

PACS: 42.55.Px, 42.60.Pk DOI: 10.1088/0256-307X/30/6/064201

Terahertz (THz) frequencies are defined as electromagnetic spectra which are located between 1–10 THz. Compared with the neighboring microwave and infrared spectral range, terahertz frequencies are technologically less developed despite the fact that they have wide-ranging applications in imaging, spectroscopy, and remote sensing.[1,2] This is largely due to the lack of convenient and efficient sources that can meet the requirement of high output optical intensity and continuous-wave (cw) operation. THz quantum cascade laser (QCL)[3] is expected to be the light source that has the most potential to satisfy those requirements. Many applications require cw operation of THz QCLs for frequency stability, which makes developing cw THz QCLs highly desired. Most cw THz quantum cascade lasers are hitherto based on double-sided metal waveguide due to the better performance about threshold gain and heat removal.[4] However, lasers with double-sided metal waveguides are generally accompanied by lower output power and larger divergence angle. The goal of obtaining high-power and controlled beam quality in cw THz QCLs is always pursued. Compared with double-sided metal waveguides, the mode of semi-insulating (SI) surface-plasmon waveguides extends substantially into the substrate, a larger mode size results in a less-divergent beam, smaller impedance mismatch at the cavity facet leads to a more favorable ratio of mirror losses which yields higher output powers and efficiencies.[5] In this Letter, we realize high performance cw QCLs at 3.2 THz based on a bound-to-continuum active region integrated SI surface-plasmon waveguide. It is a robust structure for higher power THz quantum cascade lasers operating above liquid nitrogen temperature in cw mode.

Our laser structure is based on GaAs/$Al_{0.15}Ga_{0.85}$As heterostructure, which is similar to Ref. [6] except that all layer thicknesses are expanded approximately 2%. The wafer is grown by EPI GENII solid source MBE on a semi-insulating GaAs substrate. The SI surface-plasmon waveguide is adopted to provide modal confinement. Samples are processed into 130 μm and 230 μm ridge stripes by optical lithography and wet chemical etching (H_3PO_4:H_2O_2:H_2O = 1:1:6) to the bottom contact layer. Two 20-μm-wide ohmic contact stripes of Au/Ge/Ni/Au (26/54/15/100 nm) are deposited along the edges of each ridge, and two bottom 220-μm-wide contacts are evaporated on both sides of the ridge stripes with 55-μm-wide separations between the metal on the side and the edge of the ridge. Thermal annealing for 15 s at 390℃ under nitrogen atmosphere follows to provide ohmic contact. Ti/Au is deposited on top of the laser bars as well as on the selective areas of the bottom contact layer to provide the confinement and to allow for wire bonding. Then, the substrate is thinned down to ∼200 μm and Ti/Au contact is deposited on the back side. After all these steps, lasers with different cavity lengths are cleaved and an Al_2O_3/Ti/Au/Al_2O_3 high-reflectivity (HR) coating layer is evaporated on the back facet of selected devices. Finally, devices are indium soldered ridge side up on Cu heat sinks and wire-bounded.

For device measurement, the packaged laser bars are mounted on the cold finger of a vacuum He flow cryostat with polyethylene window. An $f/2.0$ Winston cone is placed right in front of the laser facet to enhance optical power collection efficiency. The light-current (L–I) characteristics are measured by a broadband thermopile power meter and a TK abso-

*Supported in part by the 100 Talents Program of Chinese Academy of Sciences under Grant No 1731110000012, the National Natural Science Foundation of China under Grant Nos 60736031, 60806018 and 60906026, and the Special-funded Program on National Key Scientific Instruments and Equipment Development under Grant No 2011YQ13001802-4.

**Corresponding author. Email: jqliu@semi.ac.cn; fqliu@red.semi.ac.cn

© 2013 Chinese Physical Society and IOP Publishing Ltd

lute THz power meter system is used to calibrate the collected optical power.

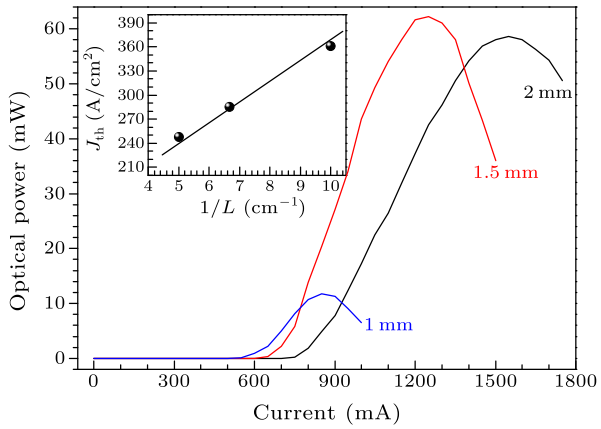

Fig. 1. Output power of the same width (130 µm) and different cavity length (1 mm, 1.5 mm, 2 mm) lasers in cw mode. The inset shows the threshold current density versus inverse laser length with back facet coating recorded at 10 K.

Device length and width are two critical factors to demonstrate high output characteristics, while longer and wider devices lead to larger gain volume but bad heat-dissipation ability which will enhance the temperature of the active region, and heat accumulation in the active region will limit the output properties severely. On the contrary, the shorter and narrower device has greater heat-removal performance which is beneficial to cw operation, while high output power is hard to demonstrate because it is restricted by small gain volume. Aiming at obtaining optimal output properties, different ridge-width and cavity-length lasers are designed. Compared with 130-µm-wide lasers, cw operation is poor for 230-µm-wide lasers due to bad heat-dissipation ability. Figure 1 shows the cw L–I characteristics of lasers with different cavity lengths at 10 K. All lasers are 130-µm-wide with the rear facet coated. The highest output optical power and slope efficiency are obtained from the 1.5-mm-long laser bar. For the 2-mm-long laser, decreasing cw output power is observed, which is contributed to severe heat accumulation in the center of the active region. For the 1-mm-long laser, lack of sufficient gain material and higher mirror loss cause an even lower optical power. The inset of Fig. 1 shows the threshold current density versus inverse laser length at 10 K. We understand from the experimental data that for the same width, the laser with longer cavity length has the lower threshold current density, which is consistent with the formula:

$$J_{\rm th} = \frac{\alpha_{\rm m} + \alpha_{\rm w}}{g\Gamma_{\rm AR}} = \frac{\alpha_{\rm w}}{g\Gamma_{\rm AR}} - \frac{\ln(R_1 \cdot R_2)}{2g\Gamma_{\rm AR}} \frac{1}{L}, \quad (1)$$

where $\alpha_{\rm m} = -\ln(R_1 \cdot R_2)/2L$ is the mirror loss, $\alpha_{\rm w}$ is the waveguide loss, g is the gain coefficient, and $\Gamma_{\rm AR}$ is the mode overlap factor with the active region, which is calculated to be 43% through our model. Assuming that the reflectivity coefficient of the cleaved facet is $R_1 = 0.32$, and the coating facet $R_2 = 1$, together with the calculated $\Gamma_{\rm AR}$, we can extract $g = 0.051\,{\rm cm/A}$ and $\alpha_{\rm w} = 2.41\,{\rm cm}^{-1}$ for 130 µm ridge width devices in cw mode from inversely proportion relation between threshold current density and inverse cavity length L.

The L–I relationship resulting from a selected 130-µm-wide and 1.5-mm-long laser bar with the rear facet coated is shown in Fig. 2. The upper panel shows the L–I–V characteristics of this laser operated at cw operation. Optical power as high as 62 mW is achieved at 10 K with a threshold current density of 285 A/cm^2. The maximum operating temperature in cw mode is 60 K. At this temperature there is still 0.16 mW optical power that can be detected. The lower panel shows optical power measured with 2 µs pulses repeated at 5 kHz for various heat-sink temperatures of the same device. The peak optical power of 64 mW is observed at 10 K and the laser lases up to 85 K. The spectrum characteristic of the laser is measured by a Fourier transform infrared (FTIR) spectrometer in rapid scan mode with a resolution of 0.5 cm^{-1}, and a DTGS pyroelectric detector is used for detection. The emission spectrum at 10 K is shown in the inset of the lower panel, which is centered on 3.2 THz.

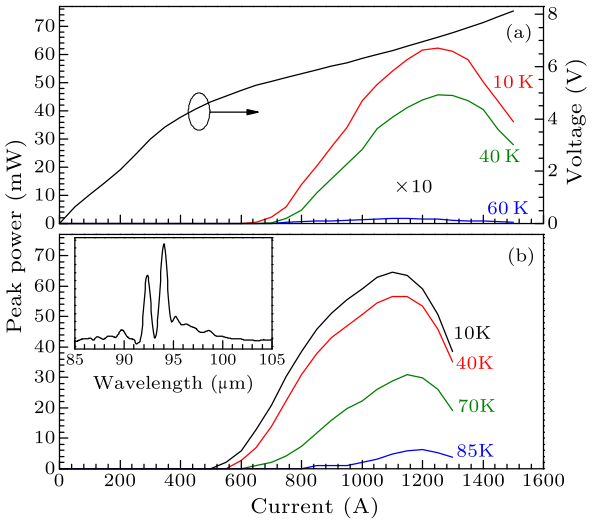

Fig. 2. L–I characteristics measured from a 130-µm-wide 1.5-mm-long ridge laser. The upper panel shows the L–I characteristics measured at cw operation and the I–V relation at various heat-sink temperatures. The lower panel shows L–I measured with 2 µs pulses repeated at 5 kHz for various heat-sink temperatures. The inset shows the spectrum of this device at 10 K.

Information from the cw and pulsed data can be used to estimate the thermal transport properties of the bonding interface. A nonlinear finite-element solver is used to model two-dimensional heat distribution in the active region and the substrate. The

bottom of the heat-sink is set to 60 K, and a heat source of 2.87×10^6 W/cm^3 is distributed uniformly across the active region in order to simulate cw operation at $T_{\max,\mathrm{cw}}$. The thermal conductivity of the active region is assumed to be $\kappa_{\mathrm{active}} = 0.5$ W/cm·K.[7] Temperature dependence of the thermal conductivity for the GaAs substrate and high doped GaAs layer are $\kappa = 745T^{-1.3}$ and $\kappa = 580T^{-1.3}$, respectively.[8] The results are shown in Fig. 3, the simulated maximum active region temperature is 80 K, 5 K lower than the measured $T_{\max,\mathrm{pulsed}}$. This discrepancy may be caused by uncertainty of the thermal conductivity values used in our model or poor bonding quality between GaAs substrate and Cu heatsink. By considering the active region as a lumped element and assuming that lasing ceases when the active region temperature $T_{\mathrm{active}} = T_{\max,\mathrm{pulsed}} = 85$ K, we can estimate the active region thermal resistance $R_T = (T_{\max,\mathrm{pulsed}} - T_{\max,\mathrm{cw}})/P = 2.46$ K/W, where P is the total electrical power dissipated in the device when we achieved highest cw optical power at 60 K.

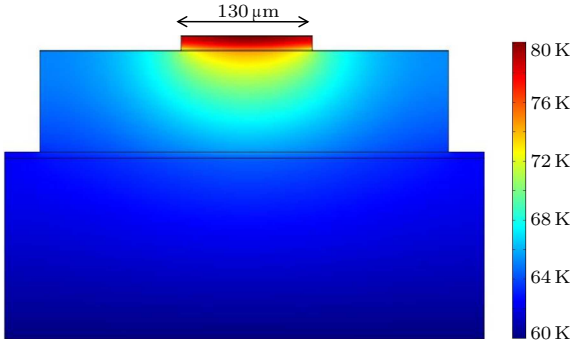

Fig. 3. Two-dimensional heat flow model calculated with a nonlinear finite-element solver. The lower boundary is set to be 60 K, and the active region is uniformly driven by a power source of 2.87×10^6 W/cm^3, which corresponds to the kink of cw optical power at the heat-sink temperature of $T_{\mathrm{sink}} = 60$ K.

Slope efficiency and wall-plug efficiency changes with the heat-sink temperature in cw operation of 130-μm-wide lasers are illustrated in Fig. 4. The slope efficiency of the laser with the rear facet coated can be written as[9]

$$\frac{dP}{dI} = \frac{h\nu}{e} N_{\mathrm{p}} \frac{\alpha_{\mathrm{m}}}{\alpha_{\mathrm{m}} + \alpha_{\mathrm{w}}} \eta_i, \qquad (2)$$

where $h\nu$ is the photon energy, e is the elemental electronic charge, N_{p} is the number of cascade period, and η_i is the internal quantum efficiency of each period. For our devices, the 1.5-mm-long bar has higher slope efficiency at all operation temperatures compared with a 2-mm-long laser. As can be seen from Fig. 4, slope efficiency drops with the increase of heat-sink temperature. The maximum value of slope efficiency we can achieve at 10 K is 156 mW/A. For the 2-mm-long device, the highest operation temperature is lower than the 1.5-mm-long one because of heat dissipation. Using the parameters obtained above, the peak internal quantum efficiency of the 150-μm-wide laser bar is 0.161 per cascade period in cw mode at 10 K. Wall-plug efficiency is defined as the peak power divided by the input electrical power. As can be seen from Fig. 4(b), wall-plug efficiency of this device has the same trend as slope efficiency with heat-sink temperature, at 10 K a maximum of 0.7% is obtained from a 1.5-mm-long laser, which is much higher than the previous double-sided metal waveguide structure.[4]

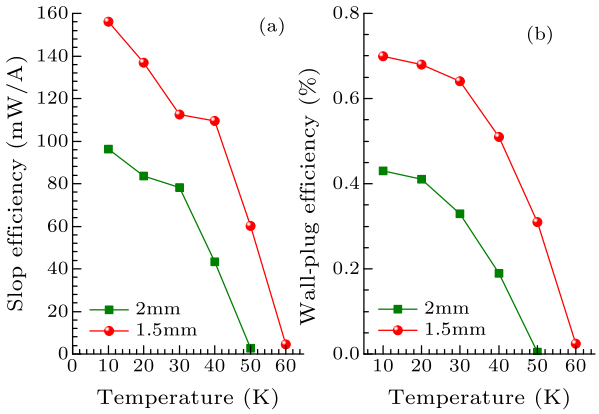

Fig. 4. slope efficiency and wall-plug efficiency as a function of heat-sink temperature for the same width (130 μm) but different cavity length (1.5 mm, 2 mm) laser bars in cw operation mode: (a) slope efficiency versus heat-sink temperature, (b) wall-plug efficiency versus heat-sink temperature.

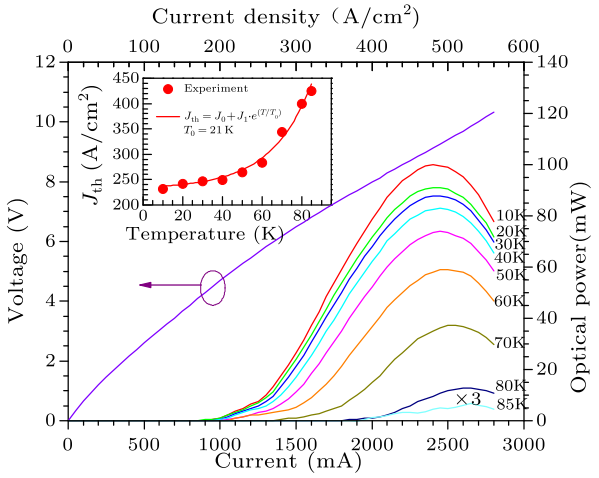

Fig. 5. Pulsed optical power as a function of injection current of a 230-μm-wide 2-mm-long device at various heat-sink temperatures. The voltage as a function of applied current at 10 K is also presented here. The inset shows the threshold current density changes with the heat-sink temperature.

For pulsed mode operation, heat accumulation is less serious compared with cw operation. Large gain material is desired to achieve higher properties. The measured optical power of a 230-μm-wide and 2-mm-long laser in pulsed mode is illustrated in Fig. 5, and

2 μs long pulses at a 5 kHz repetition rate current is used to drive our devices. The collected peak power at 10 K reaches a value of 100 mW. As shown in Fig. 5, this device can work up to a maximum temperature of 85 K, and at such a temperature we can still obtain 2.1 mW of optical power. A fit of threshold current density versus heat-sink temperature is performed to the empirical relation:[10]

$$J_{\rm th} = J_0 + J_1 \exp(T/T_0). \tag{3}$$

Such a fit is shown in the inset of Fig. 5. The characteristic temperature extracted from this fit turns out to be $T_0 = 21$ K.

In conclusion, we have achieved cw operation of terahertz quantum cascade lasers based on SI surface plasmon waveguide structure at 3.2 THz. This frequency range can be used for a bunch of practical applications such as long-range THz imaging. The maximum collected output optical power is 100 mW and 62 mW in pulsed and cw modes, respectively, at 10 K. Further optimizing the device processing and improving the heat dissipation ability, we expect to obtain more robust laser bars.

References

[1] Mittleman D M 2005 *AIP Conf. Proc.* **760** 25
[2] Siegel P H 2002 *IEEE Trans. Microwave Theory Tech.* **50** 910
[3] Kohler R, Tredicucci A, Beltram F, Beere H E, Linfield E H, Davies A G, Ritchie D A, Iotti R C and Rossi F 2002 *Nature* **417** 156
[4] Williams B S, Kumar S, Hu Q and Reno J L 2005 *Opt. Express* **13** 3331
[5] Williams B S 2007 *Nat. Photon.* **1** 517
[6] Ajili L, Scalari G, Faist J, Beere H, Linfield E, Ritchie D and G Davies 2004 *Appl. Phys. Lett.* **85** 3986
[7] Kumar S, Williams B S, Kohen S, and Hu Q 2004 *Appl. Phys. Lett.* **84** 2494
[8] Evans C A, Indjin D, Ikonic Z, Harrison P, Vitiello M S, Spagnolo V and Scamarcio G 2008 *IEEE J. Quantum Electron.* **44** 680
[9] Liu J Q, Liu F Q, Lu X Z, Guo Y and Wang Z G 2005 *Physica* E **30** 21
[10] Liu J Q, Chen J Y, Liu F Q, Li L, Wang L J and Wang Z G 2010 *Chin. Phys. Lett.* **27** 104205